# Absolute multilateration between spheres

You may also be interested in:

Uncertainty of measurement for large product verification: evaluation of large aero gas turbine engine datums
J E Muelaner, Z Wang, P S Keogh et al.

Estimation of uncertainty in three-dimensional coordinate measurement by comparison with calibrated points
J E Muelaner, Z Wang, O Martin et al.

Spectroscopically in situ traceable heterodyne frequency-scanning interferometry for distances up to 50m
Günther Prellinger, Karl Meiners-Hagen and Florian Pollinger

Geometric calibration of a coordinate measuring machine using a laser tracking system
Kenta Umetsu, Ryosyu Furutnani, Sonko Osawa et al.

Laser tracker error determination using a network measurement
Ben Hughes, Alistair Forbes, Andrew Lewis et al.

Frequency scanning interferometry in ATLAS
P A Coe, D F Howell and R B Nickerson

Towards geometrical calibration of x-ray computed tomography systems—a review
Massimiliano Ferrucci, Richard K Leach, Claudiu Giusca et al.

Air index compensated interferometer as a prospective novel primary standard for baseline calibrations
Karl Meiners-Hagen, Alen Bošnjakovic, Paul Köchert et al.

# Absolute multilateration between spheres

Jody Muelaner[1], William Wadsworth[2], Maria Azini[2], Glen Mullineux[1], Ben Hughes[3] and Armin Reichold[4]

[1] Department of Mechanical Engineering, The University of Bath, United Kingdom
[2] Department of Physics, The University of Bath, United Kingdom
[3] The National Physical Laboratory, Teddington, United Kingdom
[4] John Adams Institute for Accelerator Science, The University of Oxford, United Kingdom

E-mail: jody@muelaner.com

CrossMark

## Abstract

Environmental effects typically limit the accuracy of large scale coordinate measurements in applications such as aircraft production and particle accelerator alignment. This paper presents an initial design for a novel measurement technique with analysis and simulation showing that that it could overcome the environmental limitations to provide a step change in large scale coordinate measurement accuracy. Referred to as absolute multilateration between spheres (AMS), it involves using absolute distance interferometry to directly measure the distances between pairs of plain steel spheres. A large portion of each sphere remains accessible as a reference datum, while the laser path can be shielded from environmental disturbances. As a single scale bar this can provide accurate scale information to be used for instrument verification or network measurement scaling. Since spheres can be simultaneously measured from multiple directions, it also allows highly accurate multilateration-based coordinate measurements to act as a large scale datum structure for localized measurements, or to be integrated within assembly tooling, coordinate measurement machines or robotic machinery. Analysis and simulation show that AMS can be self-aligned to achieve a theoretical combined standard uncertainty for the independent uncertainties of an individual 1 m scale bar of approximately 0.49 $\mu$m. It is also shown that combined with a 1 $\mu$m m$^{-1}$ standard uncertainty in the central reference system this could result in coordinate standard uncertainty magnitudes of 42 $\mu$m over a slender 1 m by 20 m network. This would be a sufficient step change in accuracy to enable next generation aerospace structures with natural laminar flow and part-to-part interchangeability.

Keywords: multilateration, absolute distance measurement, coordinate measurement, ball bar, network

(Some figures may appear in colour only in the online journal)

## 1. Introduction

A major technical challenge for large scale, high value manufacturing is to provide high accuracy measurements within a factory environment, typically involving large temperature variations and line-of-sight obstructions. For example, an Airbus A350 wing is 25 m long. Over this distance positioning errors caused by the thermal expansion of tooling over a day-to-night thermal cycle of 6 °C, can be as high as 1.6 mm. Compensation for thermal expansion in complex structures with thermal gradients by using global scaling to an average temperature, as is current practice, gives little improvement. The use of multiple temperature measurements combined with thermal finite element modelling is currently being investigated [1] but not yet deployed in industrial production. Additionally typical vertical thermal gradients of 1 °C m$^{-1}$ can distort laser straightness and optical triangulation measurements over the 25 m scale by approximately 0.3 mm [2]. The next generation

of aerospace structures will require surface profile tolerances of less than 0.5 mm to achieve natural laminar flow and feature positions tolerances of less than 40 $\mu$m to achieve component interchangeability. Proving conformance with these specifications requires measurement uncertainties of the order of 50 $\mu$m over 20 m and 4 $\mu$m over 4 m respectively [3]. Measurement systems will therefore be required which are not subject to environmental disturbances in the way in which current laser tracker and photogrammetry systems are.

This paper presents an initial design of a novel measurement system that has the unique capability to provide highly accurate coordinate measurements and datum structures without being affected by the surrounding environment. It can enable a step change reduction in measurement uncertainty for large scale industrial measurement. This system is referred to as absolute multilateration between spheres (AMS).

## 2. Technical description of the ams technique

AMS uses absolute distance laser interferometry to measure the distance between steel spheres. The laser path can be mechanically shielded from local environmental disturbances and the environmental conditions of the interferometer path can be measured. Most of the spheres' surfaces are exposed in order to provide repeatable references for techniques including contact probing and scanning instruments (provided reference surfaces are coated). One possible simplified interferometer arrangement is illustrated in figure 1. The laser source is directly fibre coupled. Two quarter wave plates and a polarising beam splitter are used to direct the measurement beam in the interferometer first to one sphere, then the other before recombining it with the reference beam passing straight through the beam splitter. The method for determining the absolute distance has been left open since several methods can be considered, as is explained later. A similar approach is used in laser ball bars, most noticeably the recent Etalon Lasertracer-MT, which employs differential interferometry to measure the relative displacements of a steel sphere and a retroreflector, which move relative to one another [4]. There is no record of research for laser based absolute distance measurement between two spheres.

Reflection from the surfaces of the spheres will result in a highly divergent beam and greatly reduced throughput. Lenses located close to each sphere could prevent this divergence but would introduce additional alignment degrees of freedom which would be difficult to self-align. Analysis presented in this paper shows that measurement is possible without lenses.

The technique adopted here allows taking multiple absolute distance measurements (ADMs) between common reference spheres to provide coordinate measurements through a multilateration network. This configuration of the AMS technique is shown in figure 2. An extended network of spheres can then give accurate position information at multiple points over a large structure without the environmental disturbances which would affect current large scale instruments.

Typical large structures, such as aerospace assembly tools, require many individual interferometers, so considerations of
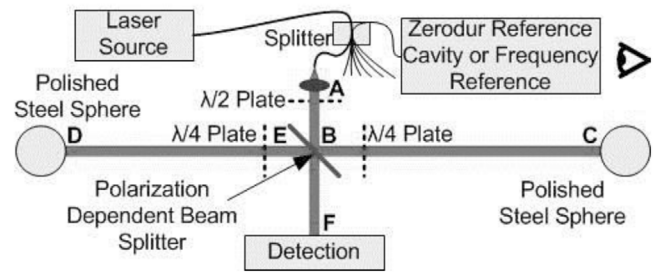


**Figure 1.** Absolute distance interferometry between two spheres with measurement path ABCDEF and reference path AF. Note that actual beam diverges over path CDEF due to curvature of spheres.

mass production and cost will be important design factors. Photonics integration technologies established for the telecoms market can enable cost-effective solutions. This has been demonstrated using frequency scanning interferometry (FSI) to provide accurate distance measurements between hundreds of targets using a dual fibre channelled laser source [5, 6]. The previous open path demonstration using FSI allowed traceable absolute distance measurements between targets; AMS will enable traceable absolute coordinates to be measured by a protected network. Using a centralised ADM laser system like FSI within AMS is one way to enable economical construction of AMS networks with hundreds of lines. The interferometer optics and detectors can be miniature, as the interferometer is only required to work along the straight line between two spheres and is held close to alignment by the environmental housing and kinematic mounts to the spheres.

The reference spheres must also be low cost and have sufficient hardness to be used as exposed references within an industrial environment. For these reasons plain metal spheres are used rather than spheres with retro-reflectors or $n = 2$ glass spheres, either of which would make the interferometer simpler. Standard industrial ball bearings are available at up to 50 mm radius with diameter tolerance of 0.13 $\mu$m, sphereicity tolerance of 0.08 $\mu$m and surface roughness of less than 0.01 $\mu$m [7].

## 3. Initial specification of the interferometer

A requirement for coordinate uncertainties of the order of 50 $\mu$m over 20 m and 4 $\mu$m over 4 m was stated in the introduction. A simplified 2D network of triangles as shown in figure 3 was simulated to determine how scale bar length measurement uncertainties propagate to give coordinate uncertainties. A Monte Carlo Method was used in which each nominal length was perturbed by an uncertainty in the central reference system and an independent random uncertainty. For each Monte Carlo iteration the coordinates were found by intersecting the lengths.

Different combinations of uncertainty in the central reference system (resulting in a consistent scale error across the network) and repeatability (from independent random uncertainties in each scale bar) were simulated. Uncertainties in the central reference system ranging from 0.05 $\mu$m m$^{-1}$ to 5 $\mu$m m$^{-1}$ were considered together with repeatabilities between 0.3 $\mu$m and 7 $\mu$m. It was found that 1 $\mu$m m$^{-1}$ standard uncertainty
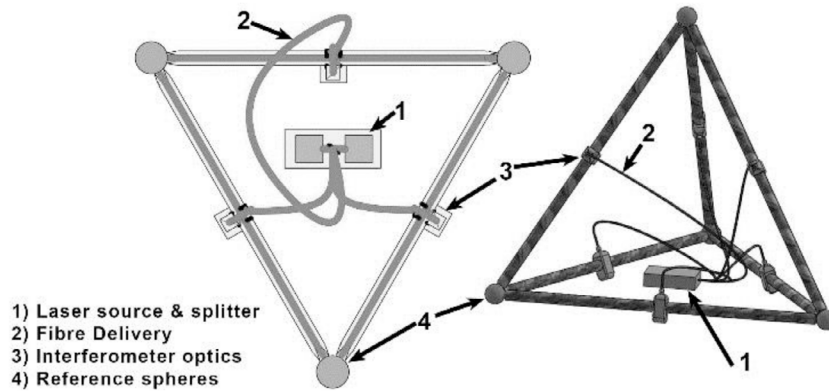
**Figure 2.** Multiple interferometers measuring common spheres to give coordinate measurements; absolute multilateration between spheres (AMS).
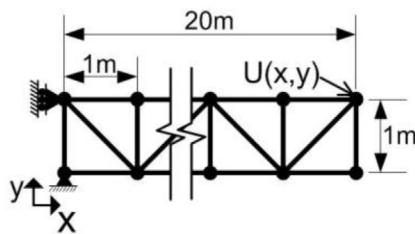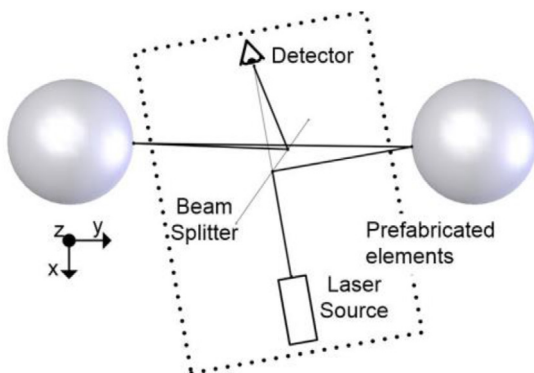


**Figure 3.** 2D network.



**Figure 4.** Simplified 2D interferometer diagram showing opposing translation and rotation errors with locally maximal power at detector, the prefabricated elements are shown (not to scale) within a dashed-line box.

in the central reference system and 0.5 $\mu$m repeatability in each scale bar would give standard coordinate uncertainties (magnitudes) of 6 $\mu$m at 4 m and 42 $\mu$m at 20 m. 1 $\mu$m m$^{-1}$ is realistic since [8] frequency scanning interferometry (FSI) has been shown to measure an absolute distance to 0.4 $\mu$m m$^{-1}$ at a 95 % confidence level with a commercial instrument [6].

Simulation was used to specify the AMS interferometer so that it would achieve the required accuracy while considering other critical performance parameters:

- **Measurement integration time:** In order to operate within an industrial environment the measurement sampling duration must be significantly shorter than any vibrations within the environment with an amplitude of the order of the laser wavelength.
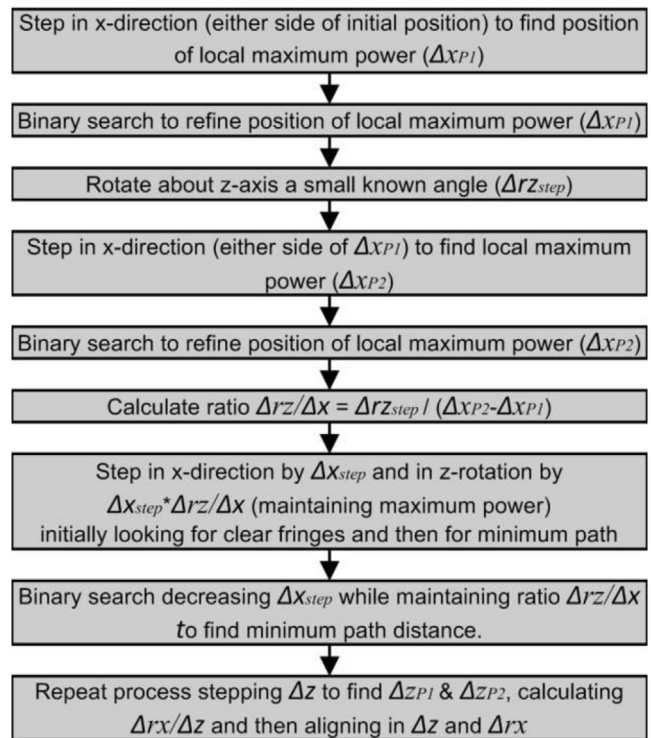


**Figure 5.** Alignment process.

- **Signal to noise ratio:** Due to the divergent nature of the measurement path the laser throughput will be low, consideration of signal to noise ratio (SNR) is therefore critical to this design.
- **Fringe contrast:** Due to beam divergence the wave front at the detector of the measurement beam will have a finite radius resulting in circular fringes across the detector. For fringes to be readily detectable there must be less than approximately 0.5 fringes across the detector. Within the analysis this is stated as the *range in optical path* for rays reaching the detector.
- **Throughput:** In order to maintain an acceptable SNR throughput, defined as the fraction of available light in the measurement beam that reaches the detector, should be sufficient.

**Figure 6.** Effect of the interferometer design parameters on the *Error Tolerance* for self-alignment (the maximum initial miss-alignment condition from which self-alignment is still possible). In each of the three 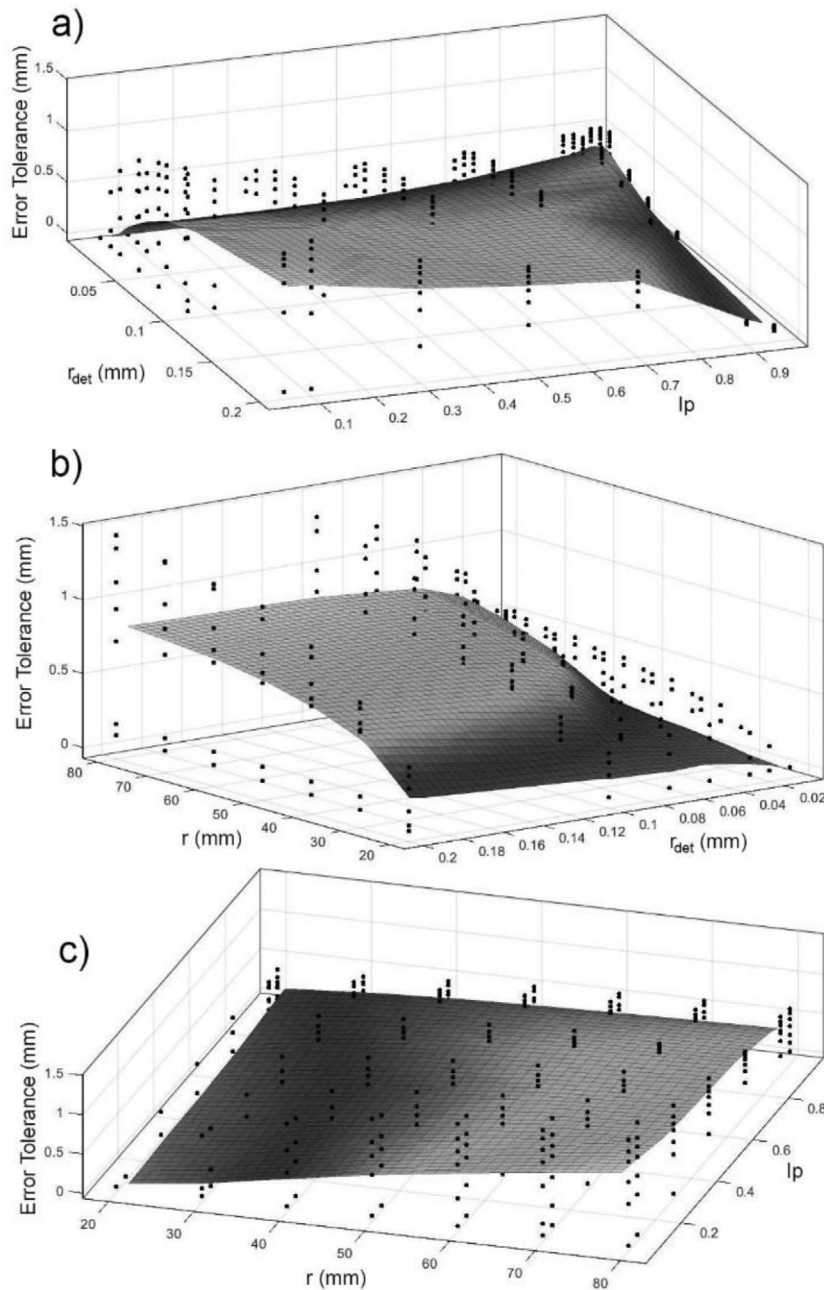plots the same data set is used with the three design parameters (*r*, $r_{det}$ and *Ip*) resulting in a different *Error Tolerance* for each point in the parameter space. Each fitted surface shows the general effect of two design parameters plotted on the *x* and *y* axes with the vertical spread of the data points giving a general indication of the effect of the third parameter a) The effect of beam splitter position (Ip) and detector radius (rdet). b) The effect of the sphere radius (r) and detector radius (rdet) c) The effect of the sphere radius (r) and beam splitter position (Ip).

- **Sensitivity to alignment errors:** Small alignment errors within readily maintainable tolerances should not increase distance measurement errors significantly or impact on other performance parameters.
- **Mechanical considerations:** The packaging of components, thermal expansion and accessibility of the sphere's surfaces as external references must be considered in the interferometer specification.

Vibrations were measured on industrial machines using a laser vibrometer with the worst conditions involving movements of $\pm 4$ $\mu$m at maximum velocities of 1 mm s$^{-1}$. In order

to count fringes, assuming a wavelength of 1550 nm, AMS must therefore sample at a rate of at least 2 kHz.

Considering photon shot noise as a potential limiting factor, the number of photons in the measurement arm ($N_m$) and reference arm ($N_r$) are given by

$$N_m = \frac{t\,T\,P\left(1 - \frac{1}{r_e}\right)}{E} \tag{1}$$

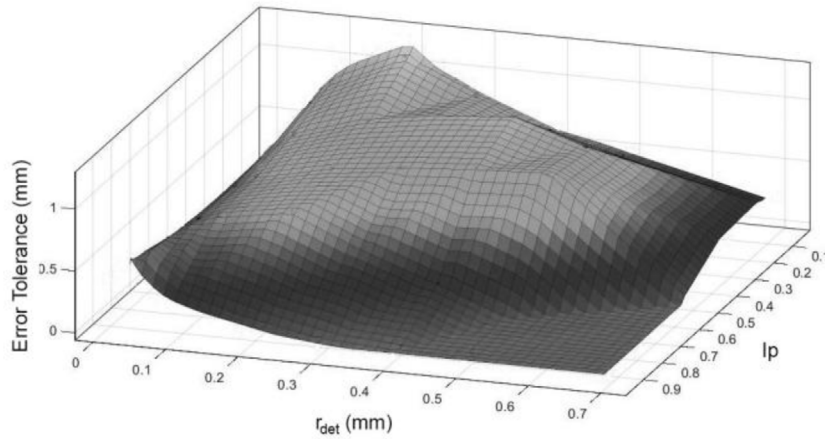$$N_r = \frac{t\,{}^{P}\!/_{r_e}}{E} \tag{2}$$

**Figure 7.** Final Optimization for $r_{det}$ and $Ip$ showing optimum configuration with 0.2 mm radius detector ($r_{det} = 0.2$ mm) and the beam splitter as close to the first sphere as possible ($Ip = 0.05$),

where $t$ is the sample time, $T$ is the throughput of the measurement arm, $P$ is the laser power, $r_e$ is the beam splitter ratio and $E$ is the photon energy.

For interferometric measurements, assuming negligible noise from the electronic circuit, the SNR is then given by

$$\text{SNR}_\text{I} = \frac{2\sqrt{N_\text{m}N_\text{r}}}{\sqrt{N_\text{m} + N_\text{r}}} \qquad (3)$$

For example, with a 10 mW 1550 nm laser, a splitter ratio of 500:1, a sample time of 0.01 ms and a throughput of $10^{-10}$ the SNR would be 18 indicating that a detectable measurement signal is possible with very low throughput. The minimum throughput, after alignment, for system design was set at $10^{-9}$ giving a SNR of 56.

For detection of power in the measurement arm, also assuming negligible electronic noise, the SNR is given by

$$\text{SNR}_\text{P} = \sqrt{N_\text{m}} \qquad (4)$$

When using the signal power during initial alignment significantly longer sample times are acceptable, with a 10 mW laser, a splitting ratio of 500:1, a sample time of 10 ms and a throughput of $10^{-11}$ the SNR is 88.

A model describing the path of a ray within the interferometer and a numerical integration algorithm using the ray model to describe the complete interferometer performance were developed. These are described in detail in section 5.

The models were used to optimize detector radius ($r_{det}$), sphere radius ($r$) and splitter position ($Ip$) for maximum throughput while maintaining a single fringe across the detector. The splitter position is defined as the distance of the centre of the beam splitter (**B**) from the surface of sphere 1 (**C**) as a proportion of the distance between the sphere surfaces (**CD**). It is therefore a number between zero and one.

Consideration was also given to thermal expansion, sensitivity to alignment errors, packaging limitations and external referencing of the spheres' surfaces. Sensitivity to alignment errors was found to be complex and could only be meaningfully considered when the alignment process was first simulated.

It is assumed that the fibre coupled laser source, beam splitter and detector are manufactured as a miniaturized
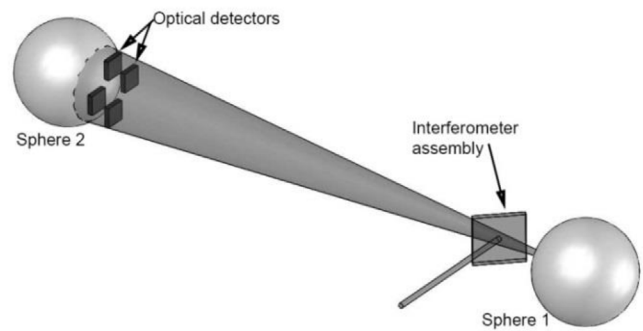


**Figure 8.** Initial alignment to second sphere.

photonic component with negligible internal alignment errors. Controlling this interferometer assembly in four degrees of freedom (DOF) would then enable alignment between the spheres. The four degrees of freedom are translation in $x$ ($\Delta x$) and $z$ ($\Delta z$), and rotation about $x$ ($\Delta rx$) and $z$ ($\Delta rz$) according to the coordinate system shown in figure 4.

In the presence of initial misalignments greater than a few micro metres, fringes across the detector prevent detection of an interference signal. Power at the detector must therefore be used for initial alignment. Perfect alignment might be expected to result in maximum power at the detector enabling a relatively simple alignment process; however, it was found that local maxima occur with opposing translational and rotational errors. It is therefore possible to find a local maximum power while there are significant errors in the measured path, as shown in figure 4.

An alignment process was devised where the central interferometer assembly is moved in a series of discrete steps (of $\Delta x_\text{step}$) in the $x$-direction until the local maximum power is found at $\Delta x_{P1}$. The interferometer assembly is then rotated by a single small known angle about the $z$-axis ($\Delta rz_\text{step}$) and subsequently moved again in the $x$-direction to find a second local maximum power, which will be approximately equal to the first power as in figure 4, at $\Delta x_{P2}$. The rotation about the $z$-axis ($\Delta rz_\text{step}$) divided by the distance in the $x$-direction between the two maximum power locations ($\Delta x_{P2} - \Delta x_{P1}$) gives a ratio of the sensitivities of the return power to these two degrees of freedom. This ratio remains constant so that it is now possible

**Table 1.** Uncertainty budget for independent uncertainties for an individual scale bar.

| Source | Value | Dist. | Divisor | Sensitivity | Standard uncertainty ($\mu$m) |
|---|---|---|---|---|---|
| Alignment | 0.05 $\mu$m | Normal | 1 | 1 | 0.050 |
| Sphere diameter | 0.13 $\mu$m | Rectang. | 1.732 | 1 | 0.075 |
| Sphere sphereicity | 0.08 $\mu$m | Rectang. | 1.732 | 1 | 0.046 |
| Sphere temperature | 0.1 | Normal | 1 | 1.25 $\mu$m °C$^{-1}$ | 0.125 |
| Sphere CTE | 1.00 $\mu$m/m/°C | Normal | 1 | 0.3 m °C | 0.300 |
| Air temperature | 0.1 °C | Normal | 1 | 0.94 $\mu$m °C$^{-1}$ | 0.094 |
| Air pressure | 100 Pa | Normal | 1 | $2.65 \times 10^{-03}$ $\mu$m Pa$^{-1}$ | 0.265 |
| Air humidity | 0.90 % | Normal | 1 | $8.73 \times 10^{-03}$ $\mu$m %$^{-1}$ | 0.000 |
| Air $CO_2$ | 200 ppm | Normal | 1 | $142 \times 10^{-06}$ $\mu$m ppm$^{-1}$ | 0.028 |
| Glass thickness calibration | 0.3 $\mu$m | Normal | 1 | 0.6832 | 0.205 |
| Glass CTE (assume 10%) | 1.00 $\mu$m/m/C | Normal | 1 | 0.020496 m C | 0.020 |
| Glass temperature (expansion) | 0.07 °C | Normal | 1 | 0.0048 $\mu$m °C$^{-1}$ | 0.000 |
| Glass temperature (index change) | 0.07 °C | Normal | 1 | $50 \times 10^{-06}$ $\mu$m °C$^{-1}$ | 0.000 |
| | | | | Combined standard | **0.49** |
| | | | | Expanded ($k = 2$) | **0.98** |

to index in *x*-translation and *z*-rotation simultaneously while maintaining maximum power. At each position the interferometer is used to try and observe fringes which will only be possible once the range in optical path is small enough. The two degrees of freedom can then continue to be moved together to a positon where the path as measured by the interferometer is minimized. The process is then repeated for the remaining two alignment errors ($\Delta z$ and $\Delta rx$). The alignment process is described in more detail by figure 5. This is intended to be a self-alignment process in that the feedback required to minimise initial alignment errors and to determine the uncertainty of the residual errors is inherent to the signals within the interferometer. The actual actuation of the central interferometer assembly in four degrees of freedom could be achieved either manually or automatically using this feedback.

There are two limiting factors for the alignment process. The first limiting factor is the throughput at the local maxima found when aligning the first two degrees of freedom; this must be a detectable signal which is assumed to be a throughput of at least $10^{-11}$ as explained above. The second limiting factor is the fringe contrast (range in optical path) when aligning the first two degrees of freedom; this must give a detectable fringe signal over a sufficient range to find the minimum path. The alignment process aligns first in one plane (translation in *x* and rotation about *z*) and then in the other plane (translation in *z* and rotation about *x*). This means that when alignment in the first plane is being carried out the initial errors in the second plane are present throughout the alignment. For self-alignment to be possible there must be a clearly detectable signal, both in terms of power and fringe contrast, when the alignment errors in the first plane are set to zero but the alignment errors in the second plane are at their initial values.

The initial values for the starting alignment involve the translation $\Delta z$ which could be positive or negative and the rotation $\Delta rx$ which could also be positive or negative. It was shown that the worst case is when $\Delta z$ is of the opposite sign to $\Delta rx$. It was also shown that when the magnitude of $\Delta rx$ in degrees

is approximately 11% of the magnitude of $\Delta z$ in mm they have a similar effect on throughput and fringe contrast. Therefore a single variable 'Error Tolerance' was defined with a value equal to $\Delta x$ and with the other misalignments set to equivalent values: $\Delta z = \Delta x$, $\Delta rz = -0.11 \Delta x°$ mm$^{-1}$ and $\Delta rx = -0.11 \Delta x°$ mm$^{-1}$ where these values are at their maximum for self-alignment to succeed. The effect of sphere radius ($r$), detector radius ($r_{det}$) and beam splitter position ($Ip$) on this Error Tolerance were investigated with the results shown in figure 6.

Increased sphere radius is clearly beneficial as might be expected since increased radius means reduced beam divergence and therefore improved throughput with increased fringe contrast. For improved interferometer performance the sphere size should be maximised which is also beneficial in terms of packaging components and providing external reference surfaces. Thermal expansion of the spheres will however increase uncertainty of measurement as the radius increases. The maximum radius ($r_{max}$) is then given by

$$r_{max} = \frac{U_{max}}{2 \, UT \, CTE} \quad (5)$$

where $U_{max}$ is the maximum acceptable uncertainty arising from thermal expansion of the spheres, UT is the uncertainty in the temperature and CTE is the Coefficient of Thermal Expansion, assumed to be 12.5 $\mu$m/m/°C for steel spheres.

If the spheres' temperatures are not measured then, assuming a fairly consistent thermal offset or gradient, this will produce a global scale error across a network of AMS interferometers. The target global scale uncertainty for the complete system is 1 $\mu$m m$^{-1}$ giving $U_{max} \approx 0.2$ $\mu$m and taking UT $\approx 6$ °C. This would give a maximum sphere radius of 1.3 mm which is clearly not feasible, using Invar this could be increased to around 13 mm but this remains too small for reasonable error tolerance. If however the temperature of each sphere is measured (with UT $\approx 0.07$ °C) and compensated then the resulting uncertainty is an independent random variable for which the target for a complete scale bar is 0.5 $\mu$m giving $U_{max} \approx 0.1$ $\mu$m
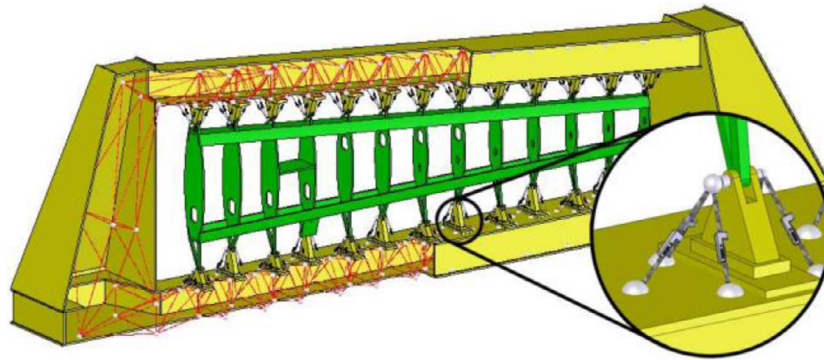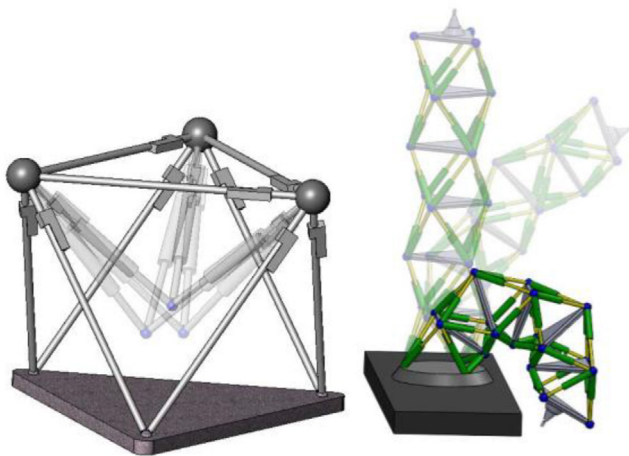
**Figure 9.** AMS embedded within a wing box assembly jig.



**Figure 10.** Dynamic AMS integrated into a CMM (left) and snake arm robot (right).



**Figure 11.** Ray path in AMS interferometer model, with an exaggerated misalignment.

and a maximum sphere radius of 57 mm. Due to availability a sphere radius of 50 mm is specified.

A second study was carried out using a fixed sphere radius of 50 mm and also considering larger detectors. The results are shown in figure 7 showing the fully optimized configuration to be spheres of 50 mm radius, a 0.2 mm radius detector and the beam splitter positioned 50 mm from the surface of the first sphere. This gives maximum initial alignment tolerance of 1.24 mm in translation ($\Delta x$ and $\Delta z$) and 0.14° in rotation ($\Delta rx$ and $\Delta rz$). An initial pre-alignment, described below, is used to get within this starting tolerance for self-alignment. It should be noted that the orientation of figure 7 has been changed when compared to figure 6(a) in order to better illustrate the shape. The reason the shape of the surface is different is that figure 6(a) represents the best fit over a range of $r$ values (indicated by the spread of points in the $z$-axis) and this range is greater when $Ip$ is large. Figure 7 on the other hand represents a single $r$ value.

A full simulation of the alignment process described in figure 5 confirmed that this configuration could be aligned to give a path error of less than 0.05 $\mu$m and a throughput of $3.0 \times 10^{-8}$ with final minimum alignment steps of 2 $\mu$m and 10 arc seconds use to align the central interferometer assembly.

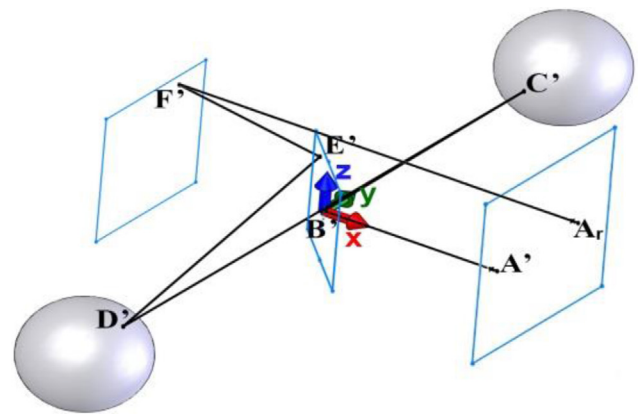Since the optimized configuration places the beam splitter only 50 mm from the surface of the first sphere it will be straightforward to maintain mechanical alignment of the interferometer assembly with the first sphere to within the 1 mm and 0.1° initial tolerance required for optical alignment. Kinematic mounts used to locate onto spherical surfaces such as tooling balls and spherically mounted retroreflectors are able to achieve mechanical alignments of around 10 $\mu$m in factory environments.

The second sphere may then be aligned to within the initial tolerance for optical alignment using a preliminary alignment process. Since the location of the interferometer assembly relative to the first sphere is determined by mechanical alignment it will be possible to synchronise translations and rotations of the interferometer to rotate the beam about the centre of the first sphere. Therefore there will be only two degrees of freedom for this alignment. A kinematic mount located on the second sphere will position an array of four optical detectors around the centre of the second sphere as shown in figure 8. These detectors will provide direct feedback to align the beam with the line between the two spheres.

A complete evaluation of the independent uncertainties for an individual scale bar is presented in table 1. The alignment uncertainty is taken directly from the above simulation. Sphere diameter and sphereicity tolerances are from the ISO standard for ball bearings [7]. Temperature, pressure and humidity sensor uncertainties are those currently achievable with low cost commercial sensors [9]. Sensitivities of the refractive index of air to environmental parameters were calculated using finite difference applied to the Ciddor equation [10, 11].

At the beginning of this section it was shown that the required network uncertainty could be achieved with a 1 $\mu$m m$^{-1}$ standard uncertainty in the central reference system and 0.5 $\mu$m standard uncertainties in the repeatability for each scale bar. The analysis presented above shows that AMS can be self-aligned to achieve this. Calibration of the sphere's CTE by dilatometry could reduce this source to a negligible level resulting in a combined standard uncertainty of 0.39 $\mu$m dominated by air pressure measurement and glass thickness calibration.

## 4. Applications for AMS

The technique of absolute distance measurement between two spheres can provide a highly accurate scale bar. Applications for such a scale bar include coordinate measurement machine (CMM) verification, scaling of photogrammetry measurements or verification of laser tracker systems. Such applications utilizing a single 1D length measurement do not however employ the complete AMS technique since they do not involve 'multilateration' between spheres.

The simplest application for the actual AMS technique is to provide a large scale coordinate reference for localized measurement systems. For example, networks of photogrammetry, laser tracker or articulated arm CMM measurements can cover large scales of 10's of metres. Such networks can also surround the object being measured so that the relative position of features on opposite sides can be measured despite these features not being accessible from any single measurement station. Unfortunately large networks lead to increased uncertainty of measurement and in uncontrolled environments this can be particularly problematic. If an AMS network is provided which surrounds the object to be measured then local measurement instruments can first reference the AMS network and then make measurements of nearby features on the object. This can significantly reduce uncertainty of measurement.

A natural progression from using AMS as a large scale coordinate reference is to embed the reference network within production tooling such as large assembly jigs. Figure 9 illustrates the concept of an AMS network embedded within assembly tooling allowing direct monitoring of key interfaces of an aircraft wing box. This can be used to provide feedback for jig actuation; for example to compensate for thermal expansion of the assembly structure. Although this network shows some slender sections a 1 m by 20 m network was shown to be feasibly in section 3.

It may also be possible to embed AMS within machines to enable accurate positional information for measurement and dynamic control. Ball bars are an industrially proven system which demonstrates that kinematic mounts can maintain alignment while moving over the surface of a sphere. For high accuracy static measurements may still be used within such dynamic machines, allowing optical re-alignment using the iterative process shown in figure 5. Figure 10 shows a parallel kinematic CMM in which the length of three members is actuated to allow a reference sphere to probe parts and a 'snake arm' robot in which linearly actuated members rotate around

**Table 2.** AMS interferometer ray model parameters.

| Variable | Description |
|---|---|
| Dimensional configuration of the interferometer | |
| $L_{AB}$ | Distance *AB*: the distance from the laser source to the beam splitter |
| $L_{CD}$ | Distance *CD*: the distance between the surfaces of the spheres, to be measured |
| $I_P$ | Position of the beam splitter between first and second sphere as a proportion of the distance $L_{CD}$ |
| $L_{EF}$ | Distance *EF*: The distance from the beam splitter to the detector |
| $r$ | The radius of the spheres |
| Error parameters | |
| $A_y$ | Radial error of laser source in *y* direction |
| $A_z$ | Radial error of laser source in *z* direction |
| $AB_{ry}$ | Rotation of laser source about *y* axis |
| $AB_{rz}$ | Rotation of laser source about *z* axis |
| $B_{rz}$ | Rotation of beam splitter about *z* axis |
| $B_{rV1}$ | Rotation of beam splitter about a vector $V_1$, perpendicular to the *z*-axis |
| $B_N$ | Position of beam splitter in its surface normal direction |
| $C_x$ | Radial error of first sphere in *x* direction |
| $C_z$ | Radial error of first sphere in *z* direction |
| $D_x$ | Radial error of second sphere in *x* direction |
| $D_z$ | Radial error of second sphere in *z* direction |

reference spheres. In the case of the CMM a static octahedron arrangement is used to locate three spheres at the top of the machine. Three telescopic bars are then connected, one to each of the three spheres at the top and joining at a forth sphere within the interior volume of the octahedron. By actuating the three telescopic bars the forth sphere can be moved within the measurement volume to probe coordinates on the part. In the case of the snake arm robot a number of octahedra are connected in series at common triangular faces made up of static bars. In each connection the 6 connecting bars are all telescopic and actuated to enable 6 DoF motion control.

## 5. Ray model of interferometer

The simulations which were used to optimize the AMS system, described in section 3, made use of an underlying model for the path of a ray within the interferometer and a numerical integration algorithm using the ray model to describe the complete interferometer performance. These models are described fully in this section.

The path of a ray within the AMS interferometer, shown in figure 11, was modelled using vector geometry and this model was independently verified using 3D CAD software. This model assumes an infinitely thin beam splitter with no secondary reflections. If the interferometer is perfectly aligned then a ray on the measurement path travels from the laser source (**A**) to a point (**B**) on the beam splitter, then to a point (**C**) on the surface of the first sphere, then a point (**D**) on the second sphere, then a point (**E**) on the beam splitter and finally arrives at a point (**F**) on the detector. When alignment

errors are present the path **ABCDEF** becomes **A′B′C′D′E′F′** as shown in figure 11. A ray on the reference path travels from point **Ar** to interfere with the measurement path ray at point **F′**. The coordinate system was arranged so that point **B** is at the origin, the path **AB** lies along the *x*-axis, in the negative direction, and the path **BC** lies on the positive *y*-axis.

The dimensional configuration of the interferometer is described by 5 parameters for lengths **AB**, **CD** and **EF** as well as the position of the beam splitter between the spheres and the sphere radius *r*. Alignment errors are described by 11 degrees of freedom for the position and orientation of the laser, the position and orientation of the beam splitter, and the position of each sphere. All parameters are described in table 2.

Although the full error model is required for determination of the ray path it was assumed that the fibre coupled laser source, beam splitter and detector are supplied as a miniaturized photonic component with negligible alignment errors. Therefore only four alignment degrees of freedom were considered in the alignments described in the preceding sections: translation in *x* ($I_x$) and *z* ($I_z$) and rotation about *x* ($I_{rx}$) and *z* ($I_{rz}$). The equivalent sphere translations, used in the ray model, can be obtained from

$$C_x = \Delta x + L_{CD} I_{\mathrm{P}} \tan(\Delta rz) \tag{6}$$

$$D_x = \Delta x - L_{CD} (1 - I_{\mathrm{P}}) \tan(\Delta rz) \tag{7}$$

$$C_z = \Delta z + L_{CD} I_{\mathrm{P}} \tan(\Delta rx) \tag{8}$$

$$D_z = \Delta z - L_{CD} (1 - I_{\mathrm{P}}) \tan(\Delta rx) \tag{9}$$

The spheres both have radius *r*. The xyz coordinates of the centre of the first sphere ($s_1$) and the second sphere ($s_2$) are given by ($C_x$, $L_{CD}I_{\mathrm{P}} + r$, $C_z$) and ($D_x$, $L_{CD}(I_{\mathrm{P}} - 1) - r$, $D_z$) respectively. The plane of the beam splitter (**P$_{\mathbf{s}}$**) is given by a point at the origin and two vectors lying on the plane (**V$_1$** and **V$_2$**) where

$$\mathbf{V_1} = \left[ -\sin\!\left(\frac{\pi}{4} - B_{rz}\right) \ \cos\!\left(\frac{\pi}{4} - B_{rz}\right) \ 0 \right] \tag{10}$$

$$\mathbf{V_2} = \mathbf{k}\cos B_{rV1} + (\mathbf{V_1} \times \mathbf{k})\sin B_{rV1} + \mathbf{V_1}\,(\mathbf{V_1} \cdot \mathbf{k}) \\ \times (1 - \cos B_{rV1}) \tag{11}$$

The path of the ray can then be modelled since

$$\mathbf{A'} = [L_{AB} \ \ A_y \ \ A_z] \tag{12}$$

And the direction vector $\overrightarrow{\mathbf{A'B'}}$ is given by rotating the direction of $\overrightarrow{\mathbf{AB}}$ first about *y* and then about *z* by the rotational alignment errors

$$\overrightarrow{\mathbf{A'B'}} = -\mathbf{i} \begin{bmatrix} \cos AB_{ry} & 0 & \sin AB_{ry} \\ 0 & 1 & 0 \\ -\sin AB_{ry} & 0 & \cos AB_{ry} \end{bmatrix}$$
$$\begin{bmatrix} \cos AB_{rz} & -\sin AB_{rz} & 0 \\ \sin AB_{rz} & \cos AB_{rz} & 0 \\ 0 & 0 & 1 \end{bmatrix} \tag{13}$$

The intersection of $\overrightarrow{\mathbf{A'B'}}$ with **P$_{\mathbf{s}}$** then gives **B′**. The direction of the line $\overrightarrow{\mathbf{B'C'}}$ can then be found by reflecting $\overrightarrow{\mathbf{A'B'}}$ about the surface normal to the beam splitter (**N$_{\mathbf{s}}$**)

$$\overrightarrow{\mathbf{B'C'}} = 2(\overrightarrow{\mathbf{A'B'}} \cdot \mathbf{N_s})\mathbf{N_s} - \overrightarrow{\mathbf{A'B'}} \tag{14}$$

The intersection of $\overrightarrow{\mathbf{B'C'}}$ with **S$_1$** then gives two possible values for **C′** and selecting the one with the minimum *y*-coordinate gives **C′**. The direction of $\overrightarrow{\mathbf{C'D'}}$ is found by reflecting about the surface normal to **S1** at **C** and the remaining points **D′**, **E′** and **F′** are found in the same way. Since the reference ray must interfere with the measurement ray at point **F′** and it emanates from the same collimated beam the remaining point **Ar** can be found by intersecting a line with direction **A′B′** and starting at **F′** with the plane normal to **A′B′** and passing through point **A′**.

The mathematical model for the ray path was verified against the CAD model and a function coded using the model. The inputs to this function were the dimensions of the interferometer ($L_{AB}$, $L_{CD}$, $L_{EF}$ and *r*) and the error parameters ($A_y$, $A_z$, $AB_{ry}$, $B_{rz}$, $B_{rV1}$, $C_x$, $C_z$, $D_x$ and $D_z$). The outputs of the function were the coordinates of the point **F′** where the ray intersects with the detector and the length error (*dL*) of the measurement path is given by

$$dL = (\mathbf{A'B'C'D'E'F'} - \mathbf{ArF'}) - (\mathbf{ABCDEF} - \mathbf{AF}) \tag{15}$$

This function may fail in a number of ways:

1. Path BC does not intersect with sphere $S_1$
2. Path CD does not intersect with sphere $S_2$
3. Path DE intersects the plane of the detector before the plane of the beam splitter
4. Large errors in alignment of a ray with a sphere of greater than approximately 0.7*r* cause a reversal of the reflection direction.

In each of these cases the actual ray would not reach the detector, additional logic was therefore included in the coded function to prevent erroneous values being returned if any of these failure conditions occurred.

The position at the detector and path error of a ray within a larger beam is now known. This was used to determine the mean path errors, range in path errors and power in a larger beam. The beam was divided into small regions with area d*y* by d*z* and numerical integration carried out over the total area of the beam which reaches the detector. The input beam profile is assumed to be a Gaussian, with the power of each ray ($P_{\mathrm{ray}}$) given by

$$P_{\mathrm{ray}} = \mathrm{d}y\mathrm{d}zP_{\mathrm{d}}\,\mathrm{e}^{\frac{-r_b{}^2}{2 \cdot c^2}} \tag{16}$$

where *dy* and *dz* are the step sizes between each ray used for integration, $P_{\mathrm{d}}$ is the peak power density of the laser, $r_b$ is the radial position of the ray within the beam and *c* is the Gaussian RMS width of the beam.

Due to the very high divergence caused by reflection off a sequence of two spherical surfaces only a very small proportion of the rays in the original beam will reach the detector. For efficient numerical integration it is therefore necessary

to first determine the limits of the region within the original beam which will reach the detector, this was achieved using pattern searches for the corners of the rectangle containing the detector. The actual integration was then carried out within these bounds to determine the range in optical path across the detector, and hence fringe contrast, the mean path error for all rays (the measured path error), and throughput (the fraction of laser power received at the detector).

The model described above assumes an initially collimated beam, since the spherical reflection surfaces cause significant divergence this is a valid assumption if the Rayleigh range is large compared to the interferometer length. Assuming a standard telecoms laser is used with a wavelength of 1550 nm and the total path distance is 2 m then a Gaussian RMS width of the order of 1 mm gives the required Rayleigh range for the ray model to give a reasonable approximation for the beam. The ray model was compared with a Gaussian beam propagation model using the ray transfer matrices with beam width varying between 0.2 and 20 mm. The difference between the calculated ranges in path distance was less than 30 pm for all beam widths. The calculated power throughputs diverged significantly for beams widths of less than 1 mm but for larger beam widths the agreement was within 10% which is sufficient to specify the system.

## 6. Conclusions and suggestions for further work

It has been shown that absolute multilateration between spheres (AMS) is theoretically capable of enabling a step change reduction in measurement uncertainty for large scale industrial measurement. This is largely as a result of avoiding the environmental disturbances which limit current laser tracker and photogrammetry systems, and through the use of multilateration which is inherently more robust to these disturbances than angle based measurements. The accuracy of AMS is limited by the uncertainty of air pressure measurement, the calibration of the thickness of the glass beam splitter cube and the central reference system which it is assumed could readily achieve a standard uncertainty of 1 $\mu$m m$^{-1}$. This could result in coordinate uncertainties over a slender 1 m by 20 m network as low as 42 $\mu$m, an order of magnitude better than current systems within uncontrolled environments, and good enough to enable natural laminar flow and part-to-part interchangeability within large civil aircraft.

Simulation shows that self-alignment is possible, and that the significant loss of throughput inherent in the design can be accommodated. In fact significant alignment errors within the interferometer can be accommodated within the diverging beam and a combination of power and distance signals can then be used to self-align the interferometer.

Work is now required to demonstrate the interferometer experimentally and to develop the central laser system with its optical reference cavities or absolute frequency references.

There are several ways to achieve the required accuracy for the central laser reference system by stabilising or measuring the reference cavity, for example using synthesised wavelength interferometry, and using absolute frequency reference

techniques such as atomic or molecular absorption lines. Frequency references in the telecommunications frequencies range are preferable to maximise the availability of cost efficient lasers and other fibre optical equipment. Measurement traceability may be achieved through direct frequency comparison methods or through comparisons between absolutely and differentially measured length changes, the latter of which can be determined using calibrated, conventional fixed frequency interferometers. The established technique of FSI measures arbitrary unknown distances to high accuracy but the lasers required are usually costly and complex. However, a single laser system may serve many hundred or even thousand interferometer bars to reduce cost. An important design consideration is to manage the large data processing load of FSI measurements. One way of reducing the data load of FSI is by combining infrequent ADM (for example sequential poling of the interferometers in the system), with a fringe counting interferometer to provide real time tracking of coordinates. Where possible, methods should be used which provide direct traceability to primary length standards, for example using Acetylene or other absorption cells as reference wavelengths. Novel ADM approaches may also exploit the fact that each scale bar has an approximately known mechanical length which may be used to reduce the required unambiguous range of the ADM. Techniques such as synthetic wavelength interferometry [12] can then determine the exact length, and may be based on modifications to commodity telecoms lasers.

## References

[1] Maropoulos P G, Vichare P, Martin O, Muelaner J E, Summers M and Kayani A 2011 Early design verification of complex assembly variability using a hybrid—model based and physical testing—methodology *CIRP Ann.* **60** 207–10

[2] Muralikrishnan B, Sawyer D, Blackburn C, Phillips S, Borchardt B and Estler W T 2009 ASME B89.4.19 performance evaluation tests and geometric misalignments in laser trackers *J. Res. Natl Inst. Stand. Technol.* **114** 1–15

[3] BSI BS EN ISO 14253-1:1999 1999 *Geometrical Product Specifications (GPS)—Inspection by Measurement of Workpieces and Measuring Equipment—Part 1: Decision Rules for Proving Conformance or Non-Conformance with Specifications* (International Organisation for Standardization)

[4] Schwenke H and Wissmann M 2012 Measuring device, Etalon Ag *German Patent Specification* WO2012010112 A2

[5] Coe P, Howell D, Nickerson R and Reichold A 2000 *An FSI Alignment System for the ATLAS Inner Detector and Some Extrapolations Towards NLC* www.slac.stanford.edu/cgi-wrap/getdoc/slac-wp-018-ch42-Reichold.pdf (Accessed: 8 June 2011)

[6] Dale J, Hughes B, Lancaster A J, Lewis A J, Reichold A J H and Warden M S 2014 Multi-channel absolute distance measurement system with sub ppm-accuracy and 20 m range using frequency scanning interferometry and gas absorption cells *Opt. Express* **22** 24869–93

[7] ISO 3290-1 2014 *Rolling Bearings—Balls. Part 1: Steel Balls* (International Organisation for Standardization)

[8] Etalon 2008 Applied traceability www.etalon-ag.com/ (Accessed: 10 November 2008)

[9] Lewis A J, Campbell M and Stavroulakis P 2016 Performance evaluation of a cheap, open source, digital environmental monitor based on the Raspberry Pi *Measurement* **87** 228–35

[10] Ciddor P E 1996 Refractive index of air: new equations for the visible and near infrared *Appl. Opt.* **35** 1566–1573

[11] Muelaner J E 2015 Ciddor equation for refractive index of air https://uk.mathworks.com/matlabcentral/fileexchange/52204-ciddor-equation-for-refractive-index-of-air (Accessed: 21 July 2015)

[12] Groot P D and Kishner S 1991 Synthetic wavelength stabilization for two-color laser-diode interferometry *Appl. Opt.* **30** 4026–33